Signatures of Magnetic Stress Prior to Three Solar Flares Observed by RHESSI

Angela Des Jardins[1], Richard Canfield[1], Dana Longcope[1], Emily McLinden[2], Amanda Dillman[3]

[1]*Montana State University, Bozeman, MT 59717-3840, U.S.A.*, [2]*Loyola University Chicago*, [3]*Rochester Institute of Technology.*

Revised: 11-12-2008

ABSTRACT

We examine the hard X-ray (HXR) footpoint sources of three flares, as observed by RHESSI, in combination with the topology given by the extrapolation of line-of-sight magnetograms into the corona. Assuming the HXR footpoint sources are chromospheric consequences of magnetic reconnection that takes place on separators, we further assume a relationship between the build-up of energy in stressed coronal magnetic fields and the measurement of the change in separator flux per unit length. We find that the value of this quantity is larger for the separators that connect the HXR footpoint sources than the quantity for the separators that do not. Therefore, we conclude that we are able to understand the location of HXR sources observed in flares in terms of a physical and mathematical model of the topology of the active region.

1. Introduction

By combining flare hard X-ray (HXR) observations with three dimensional topological models of active region coronal magnetic fields, we can expand the available tools for understanding where solar flares occur within active regions. HXRs are a signature of the presence of high-energy electrons, which are believed to originate in magnetic reconnection. Magnetic reconnection is commonly accepted as the key physical process in the release of energy stored in stressed coronal fields. The energy available to power flares is thought to be stored in the magnetic field in the form of currents positioned near separators (Henoux & Somov 1987). Separators are the three dimensional analogs of two dimensional X-points; they are the location of reconnection in three dimensional models (Gorbachev & Somov 1988). This motivates the testable hypothesis that HXR emission is associated with the separators at which reconnection has taken place.

Our analysis of the topological location of magnetic reconnection proceeds under the following working hypothesis. In the absence of reconnection, coronal magnetic fields become stressed as the photospheric boundary slowly evolves due to the emergence of new field and horizontal flows. When a critical point is reached, this energy is released by the rapid reconnection of magnetic field lines near the separator. As a result, electrons are accelerated near the reconnection region and stream along field lines near the separator. Upon encountering the chromosphere, the electrons undergo bremsstrahlung and non-thermal HXR are emitted. Thus, HXR footpoint sources can be interpreted as the location of the chromospheric ends of newly reconnected field lines, which lie close to the separator.

Past research on energy storage prior to a flare has concentrated on non-potential signatures in vector magnetograms (i.e. Gary et al. 1987; Wang et al. 1996; Moon et al. 2000; Deng et al. 2001; Tian et al. 2002; Falconer et al. 2006; Dun et al. 2007). For example, Dun et al. (2007) calculated the daily average values of three non-potential parameters from vector magnetograms: magnetic shear angle, line-of-sight current, and current helicity of selected regions along the main neutral lines of active region 10486. They found that the three non-potentiality parameters increased at the impulsively brightening flare sites from values measured at least one day before the two large X-class flares of 28 and 29 October, 2003. Dun et al. (2007) also study the magnetic flux evolution in the brightening regions and find an increase in magnetic flux and complex proper motions concurrent and co-spatial with the increases in non-potentiality.

Another way to examine the build up of energy prior to a flare is by using the Minimum Current Corona model (MCC; Longcope 1996, 2001). The MCC model tracks the complex evolution of photospheric flux to determine the lower bound on the energy stored by this motion. Longcope et al. (2007) calculate the MCC model for the 7 November 2004 X2 flare and find that the predicted flux reconnected during the flare compares favorably with values inferred from motions of the flare ribbons and the magnetic cloud. It is not necessary, however, to do the full MCC calculation to find where within an active region energy is preferentialy stored, which is the goal of this paper. We employ a restricted form of the MCC whereby we use separators to estimate the locations of energy accumulation. We hypothesize that these two methods, the MCC model and the calculation done here, examine the same fundamental physics – the relationship between the motion of photospheric sources and the build-up of energy in the line-tied coronal field.

In order to make the connection between the energy released in solar flares and the location of energy storage in the non-potential components of the magnetic field, a magnetic field model is needed. The standard flare model, CSHKP (Carmichael 1964; Sturrock 1968; Hirayama 1974; Kopp & Pneuman 1976), describes a two dimensional morphology where energy is stored in a stressed coronal field. Rapid reconnection takes place at the X point, which divides the four field line domains, reconfiguring the coronal field and converting magnetic energy into particle acceleration, heating and kinetic energy. Since some of the electrons accelerated in the reconnection process stream along the newly formed field lines and bombard the relatively dense chromosphere in a fraction of a second, the location and timing of flare emission observed in Hα, UV and HXR is a useful link to coronal reconnection location and timing.

One way the CSHKP model can be linked to energy release is by relating the properties of two-ribbon flares observed in Hα and UV to the rate of reconnection in the corona. Here, flare ribbons are taken to be the photospheric/chromospheric intersection of the separatricies dividing the open field line domain from the closed field line domain. Due to the line-tied nature of the photospheric magnetic field, motion of the ribbon is a signature of the moving separatrix (Forbes & Lin 2000). Assuming a two dimensional field, Faraday's equation can be used to relate the uniform electric field along the reconnecting current sheet to the rate at which magnetic flux is reconnected, $E = B_n V_r$, where B_n is the normal component of the magnetic field and V_r is the apparent motion of the ribbon perpendicular to the neutral line (Forbes & Priest 1984; Forbes & Lin 2000). Thus, the electric field strength can be found using measurements of the velocity of the flare ribbons and the photospheric magnetic field. The evolution in time of this electric field during the flare gives the time profile of the reconnection rate (Qiu et al. 2002).

Here, we use HXR footpoint sources as signatures of reconnection instead of Hα or UV ribbons because the HXR footpoint sources map to the main location of energy release (Temmer et al. 2007, and references therein). Non-thermal HXR sources (above about 30 keV) are plausibly attributed to the locations where newly reconnected field lines intersect the chromosphere. Many cases of these HXR footpoint sources have been recorded over the last five years by the Reuven Ramaty High Energy Solar Spectroscopic Imager (RHESSI; Lin et al. 2002).

To examine the topological location of magnetic reconnection, we use a magnetic charge topology (MCT) model in which point sources are located on the photospheric surface (see Longcope & Klapper 2002). There are several advantages to this MCT method including: 1) Due to the fact that the topological features are quantitatively defined, powerful mathematical tools can be used. This includes the ability to calculate the magnetic flux linked by separators, which is employed in this paper. 2) The photospheric boundary of the model is a quantitative representation of the observed line of sight magnetogram. Model sources represent the flux and locations of sources in the magnetogram. The larger magnetic sources are represented by three poles, providing a quadrupolar expansion of these photospheric flux sources rather than a dipolar one. This allows us to examine internal changes and rotations of sun-spots (Beveridge & Longcope 2006). 3) Calculation of the topological features of the model coronal field is not computationally time consuming, so we are able to study how the topology evolves over time.

For the reasons given above, we use a MCT model where the sources, or *poles*, are placed on the photospheric surface. MCT models assume that the photospheric field can be partitioned into distinct unipolar regions. Also, they assume that any two field lines with both their footpoints in the same regions are topologically equivalent (Longcope 2005). As a result of the first assumption, coronal field lines are anchored in discrete flux sources separated by a contiguous region in which the normal component of the magnetic field is zero. Each coronal field line can thus be assigned to a flux *domain* according to the poles at each of its two footpoints. *Nulls* are the locations between like signed poles where the magnetic field strength is zero. The surfaces dividing these domains are *separatrix* surfaces, which intersect along *separator* field lines. A separator is the three dimensional analog to a two dimensional X point; it is the location reconnection must occur in the three dimensional MCT coronal model.

There are two alternative methods to this MCT model that also give the topology of coronal magnetic fields: the source method (e.g. Titov et al. 1993; Demoulin et al. 1994; Bagala et al. 1995; Wang et al. 2002) and quasi-separatrix layers (QSLs; for a review see Démoulin 2006). The source method represents the photospheric magnetic flux in a more complete way than is done in our model. For example, our method excludes the presence of magnetic bald patches successfully modeled by the source method. We are not, however, concerned with the modeling of bald patches, but are more interested in the powerful mathematical tools available through the use of the point-source MCT model. While our MCT method sacrifices a detailed representation of the coronal field, the calculation of QSLs *requires* its detailed structure as an input. The computation of this detailed structure is currently limited by numerical techniques. Thus, the current study of QSLs is limited to a snapshot in time (Démoulin 2006) and is not suitable for this work.

In this paper, we examine three flares that occurred within 30 degrees of disk center, were well observed by RHESSI, and had HXR footpoint sources that exhibited no motion. From Solar and Heliospheric Observatory/Michelson Doppler Imager (SOHO/MDI; Scherrer et al. 1995) line-of-sight magnetograms we obtain the topology, and thus the separators, of the active region corona through extrapolation from the poles and nulls at the photospheric boundary. We measure the flux and length associated with each separator and derive a function related to the energy stored at them. This value is related to total self current, a current that acts to prevent flux changes and thus enables the field to increase its non-potentiality. We then use the function to identify the active region separators that have the most energy. In order to determine if a short interval of the continuous energy build up phase can point to the area of the active region in which the flare HXR footpoint emissions take place, we study a three hour time period prior to each of the flares.

The paper is organized as follows. In Section 2, we discuss the HXR and magnetic field observations for the three flares in our study. Details of the analysis of the HXR footpoints and coronal topology as well as the results are given in Section 3. Finally, we give a discussion of the work in Section 4.

2. Observations

The three flares that we have analyzed were chosen because they fulfill the requirements stated above. The requirement that the flares must have occurred within 30 degrees of disk center is motivated by the fact that line of sight magnetic field beyond this range is not sufficiently close to the normal field used in the topology calculation. Secondly, the flares needed to be well observed by RHESSI so that we could make resolved images of the footpoints sources as well as be confident about the flare's basic morphology over its lifetime. For this study, we chose flares whose footpoints did not move because we wanted to be able to associate flares and separators without introducing undue complexity. The properties of the three flares are given in Table 1.

The two most commonly used RHESSI image reconstruction algorithms are Clean (Högbom 1974; Hurford et al. 2002) and Pixon (Puetter 1995; Hurford et al. 2002). Clean is an iterative reconstruction algorithm that is quick and often satisfactorally represents both point and extended sources. For these reasons, we used Clean to make the images analyzed in flares B and C. Occasionally, the Clean algorithm does not remove enough noise from an image such that the morphology of the sources is not clear. In some of these cases, the Pixon algorithm, which has superior noise reduction and photometry, can result in an image

Table 1: Flare properties.

Flare	Date	Location (heliocentric $''$)	Peak Time (UT)	*GOES* Class	AR
A	26 Feb 2004	(230,330)	02:01	X1	10564
B	6 Apr 2004	(-260, -180)	13:23	M2	10588
C	4 Nov 2004	(-280,70)	23:02	M5	10696

with sufficiently defined sources. While Pixon gives superior images, it is significantly more time consuming than Clean. For this reason, it is typically not the first choice for exploring HXR sources observed by RHESSI. Due to the low number of counts available for making an image of the footpoints of flare A, the two sources could not be distinguished from one another at the 30% level of the Clean image. Therefore, we use a Pixon image in this case.

The first flare, hereafter flare A, occurred on 26 February 2004. As can be seen in Figure 1, this flare was a *GOES* X1 class flare that had an impulsive phase lasting only a few minutes. The small peak in the RHESSI 50-100 keV emission around 01:54:30 UT is the only time it was possible to make an image of the HXR sources in this energy range. Detailed spectroscopic analysis of the flare has shown that the 25-50 keV counts after about 01:58 UT are primarily thermal in nature. The contours used to classify the flaring separators for flare A are drawn at the 20% level of a 30-100 keV Pixon image. The image, shown in Figure 2, was made by summing the counts in detectors 1-9 from 01:54:40-01:55:00 UT in the 30-100 keV range.

The second flare, hereafter flare B, took place on 6 April 2004. Flare B, an M2 class flare, was a typical mid-sized flare with a single X-ray loop and an impulsive phase lasting on the order of 10 min. The image used here was made with the Clean algorithm by summing the HXR counts in detectors 4-8 from 13:22:40-13:23:20 UT in the 25-50 keV energy range. The contours used to identify the flaring separators were defined at 30% of the maximum of this image.

The third flare, hereafter flare C, took place on 4 November 2004. Flare C was a long duration M5 class flare with an impulsive phase of about 17 min. It occurred to the West of another M class flare that peaked an hour earlier in the same active region. During the second half of the impulsive phase, a third 25-50 keV HXR source appeared to the Northeast of the primary pair. Our hypothesis for the appearance of this third HXR source is discussed in Section 4. The image used in our analysis was made with the Clean algorithm by summing the HXR counts in detectors 4-8 from 23:02:00-23:05:20 UT in the 25-50 keV range. The contours used to identify the flaring separators were defined at 30% of the maximum of this image.

Based on MDI magnetograms, we calculate the topology of the coronal field based on full disk MDI magnetograms three times for each flare, two prior to the flare and one after. For flare A, which peaked at 02:01 UT, the magnetic field data were taken in 96 min. intervals at 00:03, 01:39 and 03:15 UT. The magnetograms for flare B, which peaked at 13:23 UT, were made at 11:11, 12:51 and 14:27 UT. Around the time of flare C, which peaked at 23:02 UT, MDI magnetograms were taken every minute. We noticed that subtle changes were present in data taken just one minute apart, which we attributed to noise. In order to take advantage

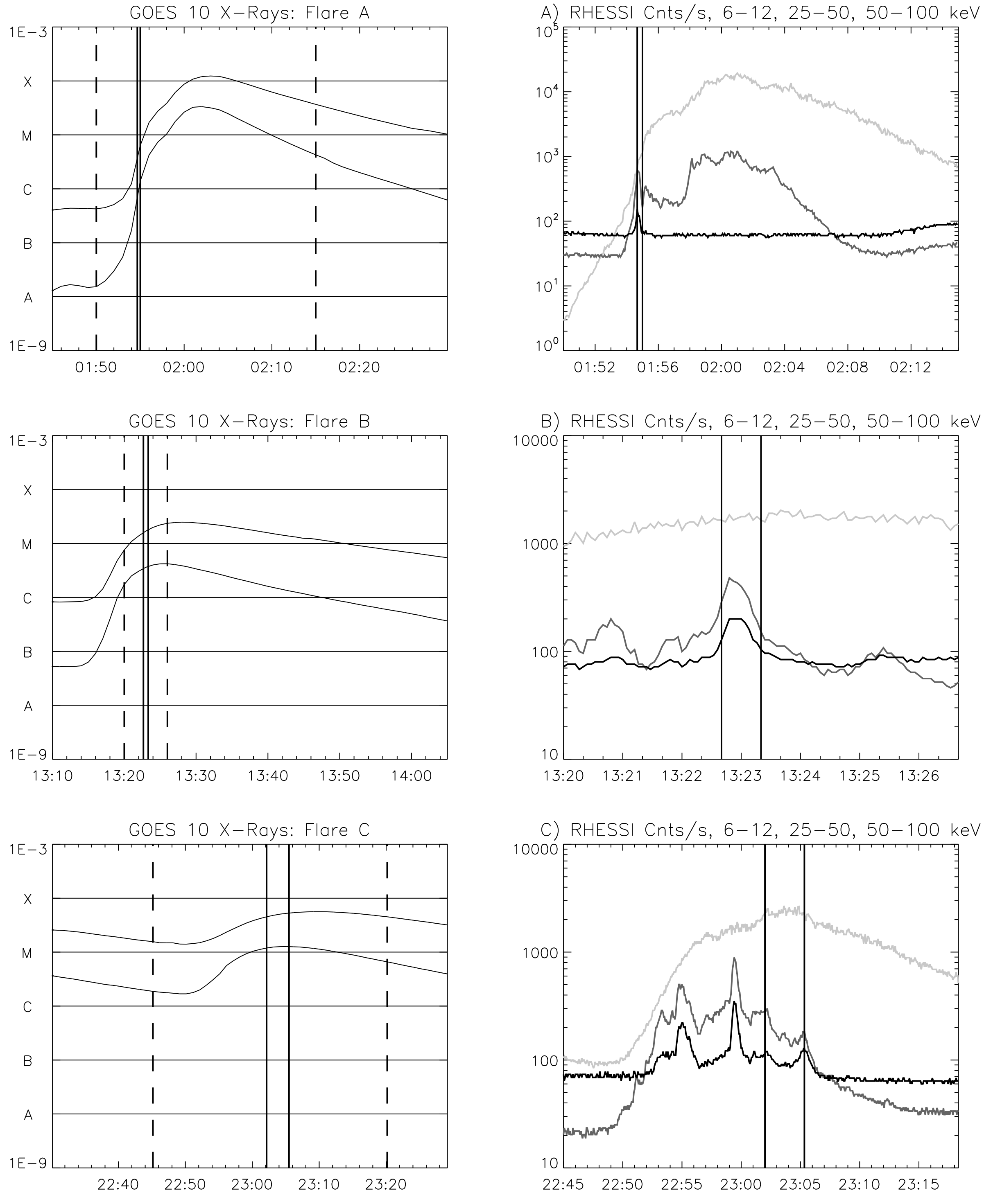

Fig. 1.— GOES and RHESSI light curves. Dashed lines in the left panels mark the time range for the right panels. The right hand panels are corrected RHESSI light curves, where the effects of attenuator and decimation state changes are accounted for. The 6-12 keV curves are light grey, 25-50 keV are dark grey and 50-100 keV are black. Solid vertical lines mark the time range over which the RHESSI images used in Figures 2 and 4 were integrated.

of the available data while decreasing the noise level, we averaged five consecutive one-minute magnetograms at 21:14-18, 22:14-18 and 23:15-19 UT. This technique of averaging over five one min. magnetograms is the same as is done on-board the spacecraft for the 96 min. magnetograms, which are used in flares A and B.

We took a straight-forward approach to the co-alignment of the MDI magnetograms and RHESSI data. Fletcher et al. (2007) report that the difference in the roll angle given in the MDI data files and the actual roll averages around 0.22 degrees, which corresponds to a combined x-y offset of $3''$ at the limb. However, we have proceeded on the assumption that the roll angle is 0 (rotated from 180 degrees in the case of flare A) and that the spatial alignment of MDI data, corrected to Earth view, and RHESSI data taken at the same time agree to within $2''$ (Krucker et al. 2005). The RHESSI data were differentially rotated to the time of the MDI observations using the SolarSoft mapping software developed by D. Zarro. While the mapping software is an approximation to the actual rotation, it is suitable for our purposes as we did not require a rotation correction of more than $\sim$2.5 hours.

3. Analysis and Results

Our analysis of the topological location of magnetic reconnection proceeds under the following working hypothesis. In the absence of reconnection, coronal magnetic fields become stressed as the photospheric boundary slowly evolves due to the emergence of new field and horizontal flows. When a critical point is reached, this energy is released by the rapid reconnection of magnetic field lines near the separator. As a result, electrons are accelerated near the reconnection region and stream along field lines near the separator. Upon encountering the chromosphere, the electrons undergo bremsstrahlung and non-thermal HXR are emitted. Thus, HXR footpoint sources can be interpreted as the location of the chromospheric ends of newly reconnected field lines, which lie close to the separator.

In order to make the connection between a flare's reconnection region and its HXR footpoints, we need to define the separators. We determine the connectivity of the field by making a model of the active region's photospheric sources observed in MDI line-of-sight magnetograms. The observed field is partitioned by grouping pixels that exceed a set threshold (100 G for flares A and B, 75 G for flare C) and are downhill from a local maximum. Regions with fewer than 10 pixels are deemed to be energetically unimportant and are discarded. Each source region with a flux less than 5×10^{19} Mx is characterized by a single point source, or pole, which matches the region's net flux and is located at the region's flux centroid. Regions with fluxes greater than 5×10^{19} Mx are represented by three poles, each with 1/3 of the region's flux, placed such that their centroid is at the same location as the region's and their quadrupole moment matches the region's. The quadrupolar expansion enables the observation of internal changes and rotations of large regions and decreases the uncertainty in the locations of topological features. A potential field extrapolated from these poles determines the locations of the topological features of the field including nulls, separatricies and separators.

As with any coronal field extrapolation model currently available, there are limitations to the MCT model we use. One limitation of our model is the loss of information on the geometry of the field. This is a result of representing patches of magnetic field with point sources. While using three point sources for the larger patches decreases the spatial uncertainty in the model, we still cannot distinguish if a coronal field line emanates from the outside edge of the modeled source or the center, for example. Another limitation of this extrapolation model is that it is potential. Currently, we do not have the ability to model coronal fields above the complex active regions where flares typically occur with a non-linear force free field model. A moderately stressed field, however, has a topology similar to that of the potential field (Brown & Priest 2000); it has the same separators dividing the flux domains. A third limitation of this MCT model is our inability to consider open field lines or sheared or twisted flux tubes, whose currents can induce significant topological changes. This means that we cannot say anything about the properties of the field at the moment of the flux tube eruption in the CSHKP model. We can, however, examine the closed field prior to and after the flare. The evidence we have for reconnection deals with electrons streaming along the closed field lines that have collapsed down beneath the separator. Using these closed field lines and the information we have from HXR emission still allows us to point to the topological location of reconnection and thus learn a great deal about the storage and release of energy in flares.

When using flare footpoints as a signature of reconnection in the corona, one of the first steps is to establish footpoint conjugacy. We have done this using three techniques. First, we compare the general characteristics (e.g. rise, peak and decay times) of the HXR light curves of the candidate pair. If the two footpoints are connected by the same field lines, then the fast electrons running down either side of those lines should impact the chromosphere within one second of each other. Second, we examine the topology model to see if a connection exists between the positive and negative magnetic sources associated with the footpoints. Third, if an extreme ultraviolet image is available during the flare time, we look for a bright loop connecting the HXR source regions. This visual connection gives credence to hot evaporated plasma having filled up the newly reconnected loop. After using these three techniques we conclude that the HXR sources used in the analysis of flares A, B and C are conjugate.

Once the separators of each flaring active region have been determined, is there evidence that energy was stored preferentially at the flaring separators prior to the flare? To answer this question, we first identified all of the separators we believed to be involved in the release of energy via reconnection based on our observational criteria. These flaring separators were assumed to be those that had both their ends within $10''$ of the defined HXR footpoint contours. We use the $10''$ extension on the footpoint contours because of the uncertainty in the locations of the chromospheric ends of the separators (nulls). When representing the larger magnetic field sources with three poles, as we do here, the typical distance between nulls is $\sim 10''$.

In order to have a precise estimate of the energy stored at every separator, we attempted to follow each individual separator by matching its nulls at one time to the next. We found, however, that we were unable to complete our analysis using only the separators we could identify as the same in consecutive topology calculations. Only a small number of separators were followable because the majority of the separators that we examined bifurcated. A bifurcation is when a separator that is present at one time is not present at the next (or vice versa). With only a small number of separators, we were not able to represent the various parts of the active region well enough to obtain meaningful energy estimates.

Since we were not able to follow individual separators directly, we grouped the separators into null group pairs (NGPs). We partitioned areas of the analyzed MDI magnetograms into null groups (NGs) such that the NG areas corresponded as closely as possible to areas of strong magnetic flux while keeping all the nulls at the ends of the flaring separators in the same NG. Every separator begins and ends at a null point and thus can be categorized by its two NGs, or its NGP. Figure 2 shows the poles, nulls and null groups as well as the footpoint contours of the three flares on the corresponding magnetograms. The use of NGPs has a further advantage over following each individual separator in that it is less biased. Using only the followable separators is biased because it ignores bifurcated separators, which are indicators of major change.

Having categorized the separators into null group pairs, we were able to analyze the separators belonging to the flaring NGPs with respect to the non-flaring ones. We sought to determine if there is evidence for energy being stored preferentially at the flaring separators. Also, we wanted to ascertain if a small time sample ($\sim$3 hours) could serve as a proxy for the changes taking place over the longer energy build-up phase prior to the flare.

To do this, we measured the flux, $\Phi^{(\mathrm{v})}$, that interconnects photospheric sources by integrating the vector potential along the path Q (Longcope et al. 2005),

$$\Phi^{(\mathrm{v})} = \int_S \boldsymbol{B} \cdot d\boldsymbol{a} = \oint_Q \boldsymbol{A} \cdot d\boldsymbol{l}. \tag{1}$$

Here, Q is the separator field line closed along the photosphere and S is some surface

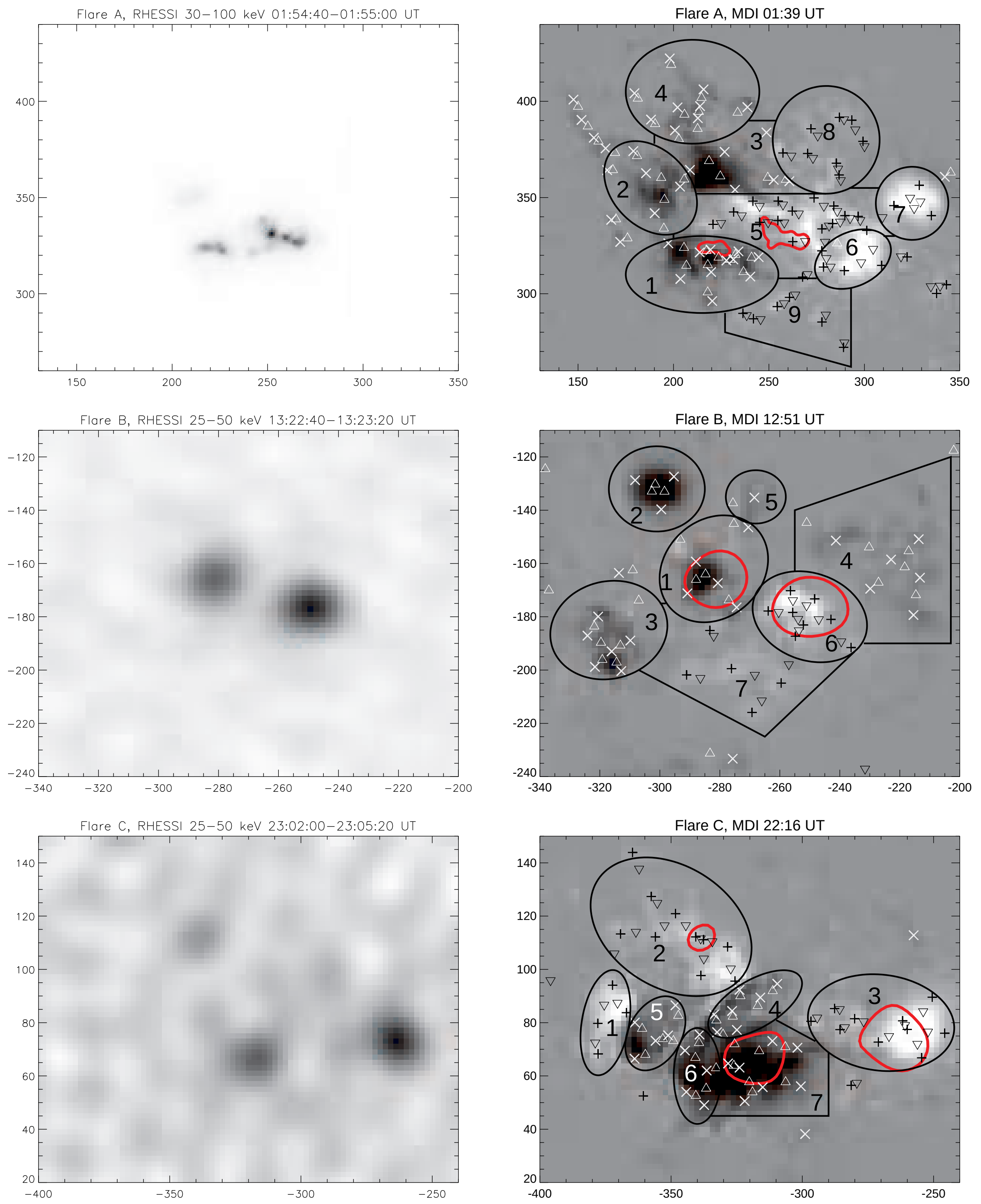

Fig. 2.— Left panels: RHESSI images used in our analysis. Right panels: MDI magnetograms with poles (+ positive, × negative), nulls (▽ positive, △ negative), null groups (outlined in black) and footpoint contours (red). Footpoint contours are at the 20% level of a 30-100 keV RHESSI Pixon image for flare A and at the 30% level of 25-50 keV RHESSI Clean images for flares B and C.

bounded by Q and line along the photosphere directly between the two nulls. Figure 3 illustrates a plausible relationship between a pole group, null group, Q, and S. We calculated this flux for every separator obtained by the model from three consecutive 96 minute MDI magnetograms, or from three averaged magnetograms one hour apart in the case of flare C. As an example, we consider null groups 3 and 7 of flare C, located in the lower right of the active region image in Figure 4. The separators connecting these null groups, shown in red, have the average flux 29 $\times 10^{11}$ Tm^2 at this time (22:16 UT). At times before and after, 21:16 and 23:17 UT, separators in the same null group averaged 12 $\times 10^{11}$ and 25.5 $\times 10^{11}$ Tm^2 respectively. We also measure the average length, l_s, of the separators in every NGP at each of the three times. The average length of the separators in NGP 3,7 of flare C at the time shown was 46 $\times 10^6$ m, and was 34 $\times 10^6$ m at the previous time, 21:16 UT and 68 $\times 10^6$ m at the following time, 23:17 UT.

We relate this flux to the energy stored at the separators by assuming that the continually changing *photospheric* magnetic field (and thus the change in separator flux) translates into a storage of energy in the *coronal* field. The flux Φ_r reconnected during the flare can be approximated as the discrepancy between the flux *actually* linked by the separator, Φ_s, and the flux linked by it in a potential field, $\Phi_s^{(\mathrm{v})}$. Prior to reconnection the flux discrepancy Φ_r = Φ_s - $\Phi_s^{(\mathrm{v})}$ changes only due to the slow, steady change in $\Phi_s^{(\mathrm{v})}$:

$$\frac{\mathrm{d}}{\mathrm{d}t}\Phi_r = -\frac{\mathrm{d}}{\mathrm{d}t}\Phi_s^{(\mathrm{v})}. \tag{2}$$

Photospheric stressing persisting steadily over a build-up time Δt_b then would build up a flux discrepancy

$$\Delta\Phi_r = -\Delta t_b \frac{\mathrm{d}}{\mathrm{d}t}\Phi_s^{(\mathrm{v})} \simeq \Delta t_b E_b l_s, \tag{3}$$

where l_s is the length of the separator. The quantity

$$E_b \simeq -(\mathrm{d}\Phi_s^{(\mathrm{v})}/\mathrm{d}t)/l_s \tag{4}$$

is one measure of how rapidly stress is building on a particular separator. It has units of electric field, but there is no electric field present during energy build-up. During reconnection, energy stored in the form of the flux discrepancy is released in the presence of an electric field, E_r over a time period Δt_r. This reconnection electric field is related to Φ_r by

$$\frac{\Delta\Phi_r}{\Delta t_r} = -E_r l_s. \tag{5}$$

Thus the separator stress, E_b, is related to the reconnection electric field by

$$E_r = \frac{\Delta t_b}{\Delta t_r} E_b. \tag{6}$$

Since we do not observe the active region over its entire build-up, we do not know Δt_b or Φ_r. We can, however, use observations over a short interval Δt to estimate the separator stress

$$E_b \simeq -\frac{1}{l_s}\frac{\Delta\Phi_s^{(\mathrm{v})}}{\Delta t}, \tag{7}$$

an approximation of definition (4). E_b is related to the current required on the separator,

$$I_s = \frac{\Phi_r}{L_s}, \tag{8}$$

where L_s is the self inductance of the loop Q, by

$$E_b = \frac{\Delta L_s I_s}{\Delta t_b}. \tag{9}$$

How the separator current, I_s, is built up prior to the flare (perhaps due to plasma motions in the flare vicinity) is a topic of interest, but will not be investigated further here.

Continuing with the above example, NGP 3,7 of flare C, we find that the change in average separator flux, $\langle\Delta\Phi_s^{(\mathrm{v})}\rangle$, from 21:15 to 22:15 UT was 17 $\times 10^{11}$ Tm^2 and the average length, $\langle l_s\rangle$, was 40 $\times 10^6$ m. When we divide $\langle\Delta\Phi_s^{(\mathrm{v})}\rangle$ by $\langle l_s\rangle$ and $\Delta t = 3600$ s, we find that $\langle E_b\rangle \simeq 12$ Vm^{-1}. Values of $\langle E_b\rangle$ for the NGPs of flares A, B and C are given graphically in Figure 4 and numerically in Table 2. In the table, E1 is the value of $\langle E_b\rangle$ calculated from differences in the first and second set of separators and E2 is from differences in the second and third.

For each flare, we have measured $\langle E_b\rangle$ for every null group pair that has at least three separators in all three analyzed topologies. (This choice is somewhat arbitrary. However, the same set of NGPs would be analyzed if we chose the NGPs with at least two separators.) We do not analyze NGPs that had two or fewer separators because the average change in flux can be completely dominated by the bifurcation of a single separator. While bifurcations are good indicators of where major change is occurring in the active region, they result in incomparable flux changes when there are only one or two separators in a group to average over. We also do not consider separators that have one or both ends at nulls that do not belong to any NG.

In Figure 4, we have plotted the nulls and separators of the calculated topology from the middle time analyzed in each flare, 01:39, 12:51 and 22:14-18 UT for flares A, B and C respectively. The group of separators shown in red in each of the panels of Figure 4 are those that had the largest separator stress $\langle E_b\rangle$. For flares B and C, the group of separators that had the largest $\langle E_b\rangle$ were the separators that were associated with the HXR footpoint sources and thus with magnetic reconnection. In the case of flare A, the largest $\langle E_b\rangle$ was not

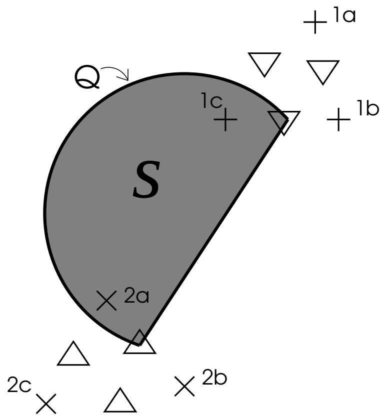

Fig. 3.— Illustration of topological features: positive poles (+) negative poles (×), nulls (▽ positive, △ negative), integration path Q and surface S.

Table 2: Values of the separator stress $\langle E_b \rangle$. Null Group Pairs (NGPs) are labeled in Figures 2 and 4. Units of $\langle E_b \rangle$ are in V m^{-1}. Ave is the average of the two measured values of $\langle E_b \rangle$. The * indicates the flaring null group pairs.

Flare A NGP	E 1	E 2	Ave	Flare B NGP	E 1	E 2	Ave	Flare C NGP	E 1	E 2	Ave
1,5*	0.73	4.91	2.82	1,6*	2.90	2.73	2.82	1,5	8.14	1.39	4.76
1,6	0.40	0.87	0.64	3,7	2.27	0.64	1.46	2,4	0.36	0.39	0.38
1,9	0.02	0.78	0.40	4,6	0.31	0.82	0.57	2,5	2.97	1.08	2.03
2,5	8.65	2.76	5.71	4,7	1.39	1.60	1.50	2,6	2.08	1.86	1.97
3,5	0.42	4.36	2.39					2,7*	0.72	4.53	2.63
4,8	0.35	0.17	0.26					3,7*	12.00	1.89	6.94

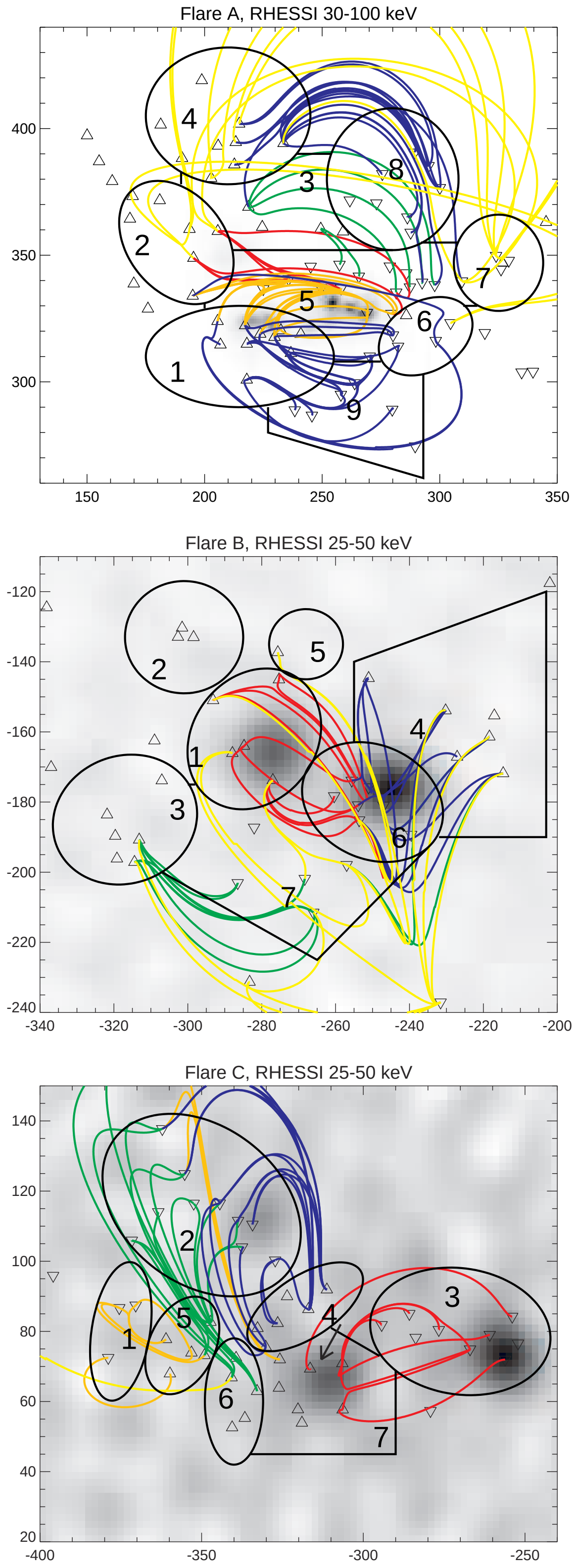

Fig. 4.— RHESSI images with null groups and separators. Separators are color coded according to average E_b, where red indicates the largest $\langle E_b \rangle$ in each flare: red = above 5 V m^{-1} (except in the case of flare B where red = above 2.5 V m^{-1}), orange = between 2.5 and 5 V m^{-1}, green = between 1 and 2.5 V m^{-1}, blue = below 1 V m^{-1} and yellow = separators not considered (see Section 3 for details).

measured in the flaring NGP 1,5, but in NGP 2,5. The flaring NGP did, however, exhibit the second largest $\langle E_b \rangle$.

4. Discussion and Conclusions

We conclude that we are able to understand the location of HXR sources observed in flares in terms of a physical and mathematical model of the topology of the flaring active region. In this paper, we have calculated the fluxes and lengths of the separators present in three flaring active regions based on MDI magnetograms and a MCT model. We studied the change in average separator flux per unit length, $\langle E_b \rangle$, where the average was over the separators belonging to the same null group pair. The function $\langle E_b \rangle$ is proportional to the self current that acts to prevent flux changes in the coronal field and is thus a signature of non-potentiality and energy storage. We find that the separator stress, $\langle E_b \rangle$, is largest for the flaring null group pair in two of the flares and is second largest in the third flare. Thus, we have shown that separators connecting the HXR sources of these flares are highly stressed.

This conclusion supports the hypothesis that the energy associated with reconnection (in the form of heating and particle acceleration) is released near separators. Prior to a flare, energy is built up in the stressed coronal field due to motions in the photospheric field. During a flare, this energy is released via reconnection at separators, resulting in the acceleration of electrons on field lines near the separator. The electrons stream along these field lines until they encounter the chromosphere and emit HXR.

In this paper, we implicitly assume that the numerical technique we use to calculate separators locates them all each time. When we attempted to follow each individual separator by matching their nulls from one time to the next, we found that a majority of the separators could not be followed. This means that either there are many separator bifurcations or our assumption about the separator locating method is not correct. We are not sure what percentage of the currently observed separator bifurcations are real and not an artifact of noise. Work is currently being done to better understand the separator locating technique.

As an example of what we consider to be real separator bifurcation, we consider the topology shown in Figure 4 for flare C. This topology does not have a separator connecting from the middle HXR source to the third footpoint (located in NG 2) which is present in the second half of flare C's impulsive phase. Several separators, however, connect the two sources in the previous and following times (at 21:15 and 23:15 UT). The bifurcation of these separators suggests a major change taking place in this area of the photospheric field, which causes the build up of stress in the coronal field above it. These connecting separators are linked to a common null (shown by the arrow) shared by the northern most flaring separator in NGP 3,7. We suggest that the third footpoint appeared because the reconnection which started on the NGP 3,7 separators triggered a secondary reconnection event, via the common null, to release energy stored at the NGP 2,7 separators.

We also conclude that the relative value of separator stress, measured for a period of time as short as 2 hours, can be used as an indicator of where within an active region a major flare is likely to occur. For the three flares studied here, which are among the largest produced by their active regions, we found that reconnection occurred at strongly stressed separators. Even in the case of flare A, which is superficially different in that more energy went into heating rather than particle acceleration, the separators of the flaring NGP were highly stressed compared to all but those in one other NGP. Hence we conclude that topological methods can reveal potential sites of major flares.

This work was supported by RHESSI funds from the University of California at Berkeley through a contract, SA1868-26308PG, with Montana State University. DWL supported by NASA grant..TBD Funding for our Research Experience for Undergraduates (REU) students was provided by NSF grant ATM-0243923.

REFERENCES

Alexander, D., & Metcalf, T. R. 1997, ApJ, 489, 442

Aulanier, G., Démoulin, P., Schmieder, B., Fang, C., & Tang, Y. H. 1998, Sol. Phys., 183, 369

Bagala, L. G., Mandrini, C. H., Rovira, M. G., Demoulin, P., & Henoux, J. C. 1995, Sol. Phys., 161, 103

Beveridge, C., & Longcope, D. W. 2006, ApJ, 636, 453

Brown, D. S., & Priest, E. R. 2000, Sol. Phys., 194, 197

Carmichael, H. 1964, in The Physics of Solar Flares, ed. W. N. Hess, 451

Démoulin, P. 2006, Advances in Space Research, 37, 1269

Demoulin, P., Bagala, L. G., Mandrini, C. H., Henoux, J. C., & Rovira, M. G. 1997, A&A, 325, 305

Demoulin, P., Mandrini, C. H., Rovira, M. G., Henoux, J. C., & Machado, M. E. 1994, Sol. Phys., 150, 221

Deng, Y., Wang, J., Yan, Y., & Zhang, J. 2001, Sol. Phys., 204, 11

Dun, J., Kurokawa, H., Ishii, T. T., Liu, Y., & Zhang, H. 2007, ApJ, 657, 577

Falconer, D. A., Moore, R. L., & Gary, G. A. 2006, ApJ, 644, 1258

Fletcher, L., Hannah, I. G., Hudson, H. S., & Metcalf, T. R. 2007, ApJ, 656, 1187

Forbes, T. G., & Lin, J. 2000, Journal of Atmospheric and Solar-Terrestrial Physics, 62, 1499

Forbes, T. G., & Priest, E. R. 1984, Sol. Phys., 94, 315

Gary, G. A., Moore, R. L., Hagyard, M. J., & Haisch, B. M. 1987, ApJ, 314, 782

Gorbachev, V. S., & Somov, B. V. 1988, Sol. Phys., 117, 77

Gorbachev, V. S., & Somov, B. V. 1989, Soviet Astronomy, 33, 57

Henoux, J. C., & Somov, B. V. 1987, A&A, 185, 306

Hirayama, T. 1974, Sol. Phys., 34, 323

Högbom, J. A. 1974, A&AS, 15, 417

Hurford, G. J., et al. 2002, Sol. Phys., 210, 61

Kopp, R. A., & Pneuman, G. W. 1976, Sol. Phys., 50, 85

Krucker, S., Fivian, M. D., & Lin, R. P. 2005, Advances in Space Research, 35, 1707

Lee, J., Gallagher, P. T., Gary, D. E., Nita, G. M., Choe, G. S., Bong, S.-C., & Yun, H. S. 2003, ApJ, 585, 524

Lin, R. P., et al. 2002, Sol. Phys., 210, 3

Longcope, D. W. 1996, Sol. Phys., 169, 91

Longcope, D. W. 2001, Phys. Plasmas, 8, 5277

Longcope, D. W. 2005, Living Reviews in Solar Physics, 2, 7

Longcope, D. W., Beveridge, C., Qiu, J., Ravindra, B., Barnes, G., & Dasso, S. 2007, Sol. Phys., in-press

Longcope, D. W., & Klapper, I. 2002, ApJ, 579, 468

Longcope, D. W., McKenzie, D. E., Cirtain, J., & Scott, J. 2005, ApJ, 630, 596

Mandrini, C. H., Demoulin, P., Henoux, J. C., & Machado, M. E. 1991, A&A, 250, 541

Metcalf, T. R., Hudson, H. S., Kosugi, T., Puetter, R. C., & Pina, R. K. 1996, ApJ, 466, 585

Moon, Y.-J., Yun, H. S., Choi, G., Park, Y. D., & Mickey, D. L. 2000, Journal of Korean Astronomical Society, 33, 47

Puetter, R. C. 1995, International Journal of Imaging Systems and Technology, 6, 314

Qiu, J., Lee, J., Gary, D. E., & Wang, H. 2002, ApJ, 565, 1335

Scherrer, P. H., et al. 1995, Sol. Phys., 162, 129

Sturrock, P. A. 1968, in IAU Symp. 35: Structure and Development of Solar Active Regions, ed. K. O. Kiepenheuer, 471

Temmer, M., Veronig, A. M., Vršnak, B., & Miklenic, C. 2007, ApJ, 654, 665

Tian, L., Wang, J., & Wu, D. 2002, Sol. Phys., 209, 375

Titov, V. S., Priest, E. R., & Demoulin, P. 1993, A&A, 276, 564

Wang, H., Yan, Y., Sakurai, T., & Zhang, M. 2000, Sol. Phys., 197, 263

Wang, J., Shi, Z., Wang, H., & Lue, Y. 1996, ApJ, 456, 861

Wang, T., Yan, Y., Wang, J., Kurokawa, H., & Shibata, K. 2002, ApJ, 572, 580